Kinetics and Catalysis, Vol. 41, No. 1, 2000, pp. 76–89. Translated from Kinetika i Kataliz, Vol. 41, No. 1, 2000, pp. 87–101.

Nonisothermal Effects in the Process of Soot Formation in Ethylene Pyrolysis behind Shock Waves

I. V. Zhil'tsova*, I. S. Zaslonko*, Yu. K. Karasevich*, and H. Gg. Wagner**

* *Semenov Institute of Chemical Physics, Russian Academy of Sciences, Moscow, 117977 Russia*
** *Institut für Physikalische Chemie der Universität Götingen, Götingen, D-37077 Germany*

Received May 19, 1998

Abstract—The nonisothermal nature of hydrocarbon pyrolysis explains the differences in the critical temperatures of soot formation in the experimental studies of these processes. When reaction heats are taken into account, the critical temperatures become close to 1600 K for all the systems studied. The estimated standard enthalpy of carbon atom formation in the composition of soot particles is $\Delta H_{f,Z} \approx 11 \pm 6$ kJ/mol. A kinetic model is proposed for soot formation in ethylene pyrolysis that describes the experimental data. The calculated temperature of soot particles may differ substantially depending on the choice of a model for energy exchange in collisions.

INTRODUCTION

Most experimental data on the kinetics of soot formation were obtained in flames and shock tubes. The main results concerning experimental measurements and the model were discussed in review papers [1, 2] and a monograph [3]. The kinetic measurements of soot formation in shock waves have well-known advantages, the majority of which are the absence of the effects of reactant diffusion and heat transfer and the possibility for varying the ratio between initial components arbitrarily. In shock tubes, the kinetics of soot formation was studied in the pyrolysis of many substances [3, 4]. The experimental findings formed the basis for constructing kinetic models, which enable the description of the following features of hydrocarbon pyrolysis:

(1) The presence of induction period τ_{ind} followed by self-acceleration;

(2) Transition to a steady-state level when the weight fraction of soot Y is approximated by the formula $Y \sim [1 - \exp(-k_{eff}t)]$, where k_{eff} is the effective rate constant of soot formation; and

(3) Low-temperature dependence of the soot yield at the steady-state level is volcano-shaped with pronounced lower and higher temperature boundaries.

The lower boundary of soot formation T_{cr} is especially interesting because (a) T_{cr} may provide information on the zones of soot formation in the combustion of diffusional flames and (b) T_{cr} enables reasoning on the main factors that initiate soot formation. Table 1 summarizes the data [5] on the values of T_{cr} in diffusional flames for various hydrocarbons. This table also presents the results of T_{cr} determination in shock waves. A substantial difference in the values of T_{cr} for different compounds and sometimes for the same compound from different sources is worth commenting on. This difference is explained by the fact that, in kinetic experiments on soot formation in shock waves, the condition of the substantial dilution of a reacting mixture with an inert gas is not always fulfilled, although dilution maintains a constant temperature. The difficulty in creating these conditions is associated with the fact that soot is formed only after reaching a threshold concentration of a hydrocarbon in the mixture; that is, $[C] > [C]_{cr}$, where $[C]_{cr} \approx (3–5) \times 10^{-7}$ mol/cm^3. Therefore, to carry out experiments under a pressure of about 1 atm, the initial mixture should be used that contains at most 1% of carbon-bearing molecules. Because soot formation occurs at high conversions, a change in temperature relative to the initial temperature may be several hundreds degrees. Such a temperature change may affect the process kinetics, and this should be taken into account when interpreting kinetic experiments.

Soot formation in CCl_4 is an eloquent example. According to Frenklach *et al.* [6], $T_{cr} \sim 2500$ K in CCl_4 pyrolysis. This value is much higher than that obtained by Starikovsky *et al.* [5] for the same process and the values for other compounds listed in Table 1. This difference is due to the fact that Frenklach *et al.* assigned the results on the soot yield to the initial temperature behind a shock wave. Since these experiments were carried out in the mixtures containing 9% of CCl_4 in Ar, a decrease in the temperature of the mixture should be substantial in pyrolysis.

Note that the main characteristics of soot formation in the pyrolysis of halogenated and nonhalogenated hydrocarbons are very close. Specifically, Table 1 shows that the values of the critical temperature for all compounds are about the same, provided that the nonisothermal nature of the processes, is taken into account. Therefore, we suggest that the mechanisms of soot formation in the pyrolysis of halogenated and nonhalogenated hydrocarbons are similar.

0023-1584/00/4101-0076$25.00

Another interesting aspect of nonisothermal soot formation is the possibility for the appearance of a difference in the temperatures of growing particles and ambient gas. The growth of soot particles is accompanied by the corresponding energy release. This energy is accumulated on the internal degrees of freedom of growing particle possibly resulting in its overheating. If growth is fast, the dissipation of evolved energy in collisions with the particles of ambient gas may not be efficient enough, and a difference in the temperatures of gas and soot particles appears.

The above conclusions may be illustrated by an experimentally observed difference in the temperatures of gas and soot near a heated support on which carbon film grew from the hydrocarbon phase in a reactor [7]. The temperature difference may reach hundreds of degrees, and this should be taken into account when describing the qualitative features of film growth. To our knowledge, there are no data on the temperatures of soot particles in the pyrolysis of hydrocarbons in shock waves, although they might be a useful source of kinetic information on particle growth.

Nonisothermal effects considered above substantially affect the whole process of soot formation. To elucidate the nature of this effect, thorough analysis of the available experimental data and the creation of the corresponding model that would quantitatively predict thermodynamic aspects of the process are necessary. The goal of this work is to develop of such a model and study nonisothermal effects considered above.

KINETIC MODEL DESCRIPTION

Choice of a model. The modeling of the soot formation process is a challenge. The model should contain a block of gas-phase reactions that provide building blocks for the formation of a carbon matrix and the mechanism for the formation of the structure of this carbon matrix.

Of all kinetic models for soot formation, the mechanism proposed and developed by Frenklach [8] is most widely used. This mechanism is based on the addition of an acetylene molecule to a growing carbon matrix with the elimination of hydrogen atoms to the gas phase. This is the so-called Hydrogen Abstraction–Acetylene Addition (HACA) mechanism. Hydrogen atoms propagate the chain and recover acetylene molecules. Another approach is based on the assumption that polyyne molecules $C_{2n}H_2$ play an essential role. This mechanism formed the basis of a model proposed by Krestinin [9]. He proposed serious thermodynamic and kinetic arguments in favor of his mechanism, and these arguments let us consider this mechanism as a possible pathway for soot formation along with the competitive HACA mechanism and motivate submitting it to more thorough analyses.

Table 1. Critical temperatures for soot formation in flames and shock waves [5]

Fuel	T_{cr}, K	
	flames	shock waves
Hydrocarbons		
Acetylene	1665	1580
Allene	1585	1600
Ethylene*	1700	1550
		1650
Benzene	1580	1600
1,3-Butadiene	1650	1600
Isobutane	1684	
Toluene	1570	1600
Methane		1650
Propane		1550
Halogenated hydrocarbons		
CCl_4	–	1680
		2500**
CH_2Cl_2	–	1580
$C_2H_2Cl_2$	–	1800
C_2HCl_3	–	1800
C_2H_3Cl	–	2000***
CH_3Cl	–	2000***
$CHCl_3$	–	2000***
C_6F_6	–	1600
CF_4	–	1700

* Upper and lower values of T_{cr} obtained in shock tubes correspond to the measurements at high and low pressures.

** Data from the experiments with mixtures containing 9.3% CCl_4 should be corrected taking into account that the gas mixture is substantially cooled because of CCl_4 dissociation before the start of the soot formation process.

*** T_{cr} obtained at high concentrations of fuel in the starting mixture; these values should be corrected for the nonisothermal nature of the process.

Description of the kinetic scheme. To model the process of soot formation taking into account nonequilibrium temperature effects, we should use a kinetic scheme for which reliable thermochemical data on the main intermediate species are available. The kinetic scheme that models the process of soot formation in acetylene pyrolysis [9] formed the basis of such a scheme. The mechanism of acetylene pyrolysis is based on the dominating role of polyyne molecules in the process of soot formation. This scheme was adapted to ethylene pyrolysis as described in Table 2.

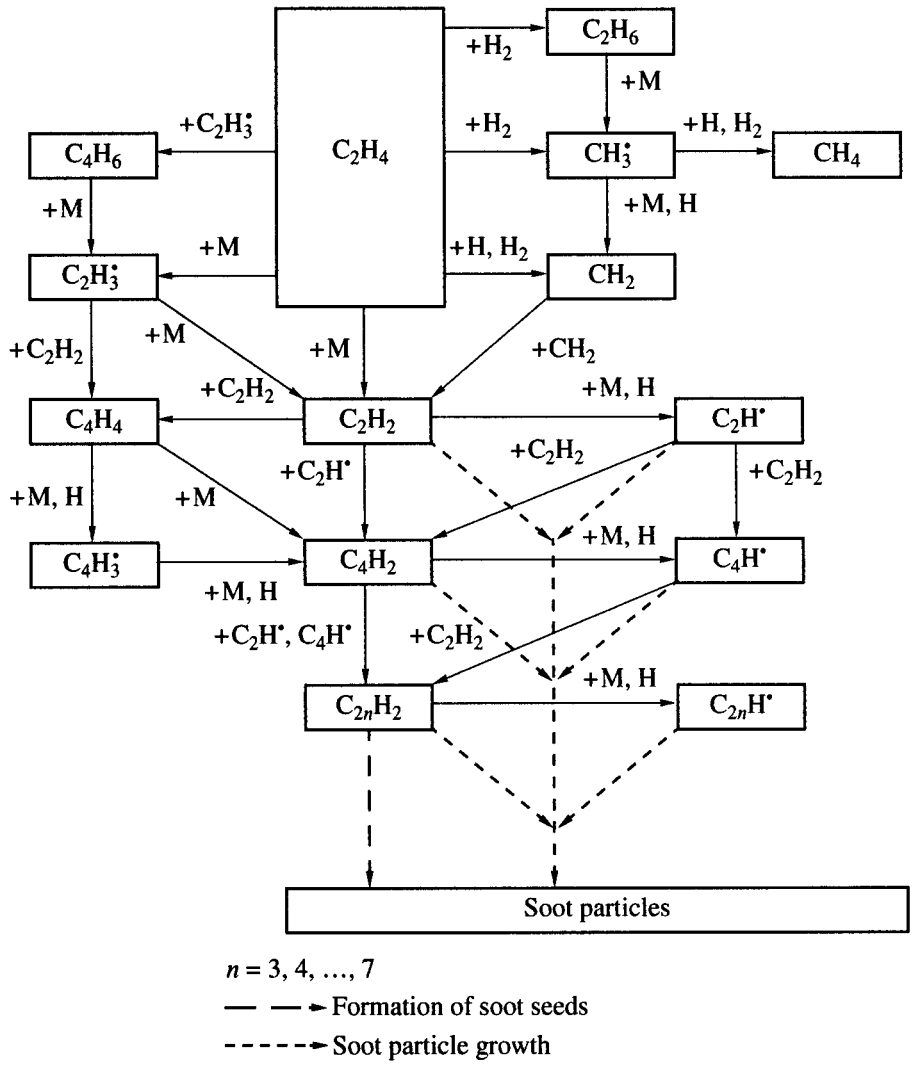

Fig. 1. Transformations of the main species in ethylene pyrolysis.

Figure 1 illustrates the sequence of transformations of the main species. Polyyne molecules are formed via the following reversible reactions

$$C_{2n}H_2 + C_2H^{\bullet} \rightleftharpoons C_{2n+2}H_2 + H,$$

$$C_{2n}H^{\bullet} + C_2H_2 \rightleftharpoons C_{2n+2}H_2 + H,$$

$$C_{2n}H_2 + C_4H^{\bullet} \rightleftharpoons C_{2n+4}H_2 + H,$$

$$C_{2n}H^{\bullet} + C_4H_2 \rightleftharpoons C_{2n+4}H_2 + H.$$

These fast radical reactions result in an increase in the concentrations of species with a high C/H ratio.

Bimolecular reactions between polyyne molecules with the elimination of molecular hydrogen lead to the formation of species with 20 carbon atoms or more. These reactions were considered to seed soot particles Z:

$$C_{2n}H_2 + C_{2m}H_2 \longrightarrow Z + 2H_2 \ (m + n \geq 20). \qquad \text{(I)}$$

A strict consideration of the properties of the condensed phase (including soot particles), which is formed during the gas-phase reaction, requires the knowledge of the function of particle distribution over sizes. However, this is a very complicated problem, and therefore various approximations are used [10]. In this work, we are restricted to the monodispersed approximation, which proved acceptable in other studies [11–13]. Within the framework of this approximation, it is only necessary to know the weight of the material formed and the concentration of the species.

The reactions of Z particles with carbon-bearing molecules and gas-phase radicals containing one or two carbon atoms ($C_{2n}H^{\bullet}$ and $C_{2n}H_2$, n = 1–7) lead to an increase in the weight of soot and the recovery of chain carriers: H, H_2, $C_2H^{\bullet}$, and C_2H_2. These reactions take the following form within the monodispersed approximation:

$$Z + C_{2n}H_2 \longrightarrow Z + H_2, \qquad \text{(II)}$$

$$Z + C_{2n}H^{\bullet} \longrightarrow Z + H. \qquad \text{(III)}$$

Table 2. Parameters of reactions included in the kinetic scheme of the soot formation process in ethylene pyrolysis

No.	Reaction	Rate constant				References
		forward reaction		reverse reaction		
		log$A$	E_a, kJ/mol	log$A$	E_a, kJ/mol	
1	$C_2H_4 + M \rightleftharpoons C_2H_2 + H_2 + M$	16.48	296.0	15.04	126.0	[31]
2	$C_2H_4 + M \rightleftharpoons C_2H_3^{\cdot} + H + M$	17.64	410.0	15.87	–7.1	[32]
3	$C_2H_4 + H \rightleftharpoons C_2H_3^{\cdot} + H_2$	14.80	71.1	13.65	90.0	[31]
4	$C_2H_4 + H \rightleftharpoons CH_3^{\cdot} + CH_2$	15.95	250.0	13.60	0	[33]
5	$C_2H_4 + H_2 \rightleftharpoons CH_3^{\cdot} + CH_3^{\cdot}$	17.37	362.0	15.67	129.0	[31]
6	$C_2H_4 + C_2H^{\cdot} \rightleftharpoons C_2H_3^{\cdot} + C_2H_2$	13.48	0	13.28	101.0	[34]
7	$C_2H_4 + H_2 + M \rightleftharpoons C_2H_6 + M$	16.04	159.0	17.36	283.0	[35]
8	$C_2H_4 + C_2H_3^{\cdot} \rightleftharpoons C_4H_6 + H$	12.38	33.6	13.66	39.7	[34]
9	$C_2H_3^{\cdot} + M \rightleftharpoons C_2H_2 + H + M$	14.68	152.0	14.39	–36.9	[31]
10	$C_2H_3^{\cdot} + H \rightleftharpoons C_2H_2 + H_2$	13.60	0	13.94	248.0	[33]
11	$C_2H_3^{\cdot} + H \rightleftharpoons CH_2 + CH_2$	15.16	285.0	13.30	0	[36]
12	$C_2H_3^{\cdot} + C_2H^{\cdot} \rightleftharpoons C_2H_2 + C_2H_2$	11.98	0	13.27	330.0	[37]
13	$C_2H_3^{\cdot} + C_2H_3^{\cdot} \rightleftharpoons C_4H_6$	12.04	5.0	15.41	361.0	[31]
14	$C_2H_2 + M \rightleftharpoons C_2H^{\cdot} + H + M$	20.00	531.0	19.43	12.0	[37]
15	$C_2H_2 + H \rightleftharpoons C_2H^{\cdot} + H_2$	13.96	95.7	13.01	13.3	[31]
16	$C_2H_2 + H_2 \rightleftharpoons CH_2 + CH_2$	16.78	316.0	13.48	0	[36]
17	$C_2H_2 + C_2H^{\cdot} \rightleftharpoons C_4H_2 + H$	13.65	0	15.03	61.4	[38]
18	$C_2H_2 + C_2H_2 + M \rightleftharpoons C_4H_4 + M$	17.45	217.0	18.59	345.0	[31]
19	$C_2H_2 + C_2H_2 \rightleftharpoons C_4H_2 + H_2$	14.00	218.0	14.43	197.0	[34]
20	$C_2H_2 + C_2H_2 \rightleftharpoons C_4H_3^{\cdot} + H$	15.54	326.0	15.80	128.0	[34]
21	$C_2H^{\cdot} + C_2H^{\cdot} \rightleftharpoons C_4H^{\cdot} + H$	14.00	0	16.48	200.0	[9]
22	$CH_2 + CH_2 \rightleftharpoons C_2H_2 + H + H$	14.30	0	15.87	96.6	Estimate
23	$CH_4 + M \rightleftharpoons CH_3^{\cdot} + H + M$	20.73	437.0	18.74	0	[31]
24	$CH_4 + H \rightleftharpoons CH_3^{\cdot} + H_2$	14.98	37.4	13.61	36.7	[31]
25	$CH_3^{\cdot} + M \rightleftharpoons CH_2 + H + M$	18.57	453.0	17.30	0	[31]
26	$CH_3^{\cdot} + H \rightleftharpoons CH_2 + H_2$	13.78	63.1	13.12	46.8	[39]
27	$CH_3^{\cdot} + CH_3^{\cdot} \rightleftharpoons C_2H_6$	12.45	–11.1	15.46	347.0	[31]
28	$C_4H_4 + M \rightleftharpoons C_4H_2 + H_2 + M$	16.52	314.0	15.84	163.0	[34]
29	$C_4H_4 + M \rightleftharpoons C_4H_3^{\cdot} + H + M$	17.50	356.0	16.64	27.2	[34]
30	$C_4H_4 + H \rightleftharpoons C_4H_3^{\cdot} + H_2$	11.60	0	11.36	108.0	[40]

Table 2. (Contd.)

No.	Reaction	Rate constant				References
		forward reaction		reverse reaction		
		log*A*	E_a, kJ/mol	log*A*	E_a, kJ/mol	
31	$C_4H_4 + H \rightleftharpoons C_2H_3^{\cdot} + C_2H_2$	13.15	–37.6	12.32	21.0	[31]
32	$C_4H_4 + C_2H^{\cdot} \rightleftharpoons C_2H_2 + C_4H_3^{\cdot}$	13.60	0	14.32	190.0	[38]
33	$C_4H_4 + C_2H_3^{\cdot} \rightleftharpoons C_4H_3^{\cdot} + C_2H_4$	13.00	60.6	13.91	150.0	[34]
34	$C_4H_4 + C_4H^{\cdot} \rightleftharpoons C_4H_3^{\cdot} + C_4H_2$	13.68	32.1	13.30	83.6	[9]
35	$C_4H_3^{\cdot} + M \rightleftharpoons C_4H_2 + H + M$	16.01	249.0	15.56	–10.3	[38]
36	$C_4H_3^{\cdot} + H \rightleftharpoons C_4H_2 + H_2$	13.91	0	14.08	178.0	[34]
37	$C_4H_2 + M \rightleftharpoons C_4H^{\cdot} + H + M$	17.82	488.0	17.34	108.0	[31]
38	$C_4H_2 + H \rightleftharpoons C_4H^{\cdot} + H_2$	13.20	5.9	13.34	62.4	[31]
39	$C_4H_2 + C_2H^{\cdot} \rightleftharpoons C_4H^{\cdot} + C_2H_2$	13.30	0	14.39	139.0	Estimate
40	$C_4H_2 + C_2H^{\cdot} \rightleftharpoons C_6H_2 + H$	13.30	0	14.00	62.7	[38]
41	$C_4H_2 + C_4H^{\cdot} \rightleftharpoons C_6H_2 + C_2H^{\cdot}$	15.23	141.0	14.30	0	[9]
42	$C_4H^{\cdot} + C_2H_2 \rightleftharpoons C_6H_2 + H$	13.60	0	14.00	66.0	[38]
43	$C_4H^{\cdot} + C_4H_2 \rightleftharpoons C_8H_2 + H$	15.54	75.4	17.61	0	[31]
44	$C_6H_4 + M \rightleftharpoons C_6H_2 + H_2 + M$	17.79	200.0	14.48	0	Estimate
45	$C_6H_2 \rightleftharpoons C_6H^{\cdot} + H$	14.90	502.0	13.11	108.0	[34]
46	$C_6H_2 + H \rightleftharpoons C_6H^{\cdot} + H_2$	14.00	86.9	13.30	0	[34]
47	$C_6H_2 + C_2H^{\cdot} \rightleftharpoons C_6H^{\cdot} + C_2H_2$	13.81	–125.0	13.60	0	[9]
48	$C_6H_2 + C_2H^{\cdot} \rightleftharpoons C_8H_2 + H$	13.60	0	14.00	62.7	[34]
49	$C_6H_2 + C_4H^{\cdot} \rightleftharpoons C_8H_2 + C_2H^{\cdot}$	13.48	135.0	14.00	0	[9]
50	$C_6H_2 + C_4H^{\cdot} \rightleftharpoons C_{10}H_2 + H$	13.30	0	14.00	66.0	[9]
51	$C_6H_2 + C_4H_3^{\cdot} \rightleftharpoons C_6H^{\cdot} + C_4H_4$	13.30	83.6	12.38	18.6	[9]
52	$C_6H_2 + C_6H^{\cdot} \rightleftharpoons C_{12}H_2 + H$	13.60	0	14.00	66.0	[9]
53	$C_6H^{\cdot} + C_2H_2 \rightleftharpoons C_8H_2 + H$	13.60	0	14.00	66.0	[34]
54	$C_6H^{\cdot} + C_4H_2 \rightleftharpoons C_{10}H_2 + H$	13.30	0	14.00	66.0	[9]
55	$C_8H_4 + M \rightleftharpoons C_8H_2 + H_2 + M$	17.70	209.0	14.48	0	Estimate
56	$C_8H_2 \rightleftharpoons C_8H^{\cdot} + H$	14.90	502.0	13.43	30.1	[34]
57	$C_8H_2 + H \rightleftharpoons C_8H^{\cdot} + H_2$	14.00	86.9	13.30	0	[34]
58	$C_8H_2 + C_2H^{\cdot} \rightleftharpoons C_8H^{\cdot} + C_2H_2$	13.51	–47.2	13.60	0	[9]
59	$C_8H_2 + C_2H^{\cdot} \rightleftharpoons C_{10}H_2 + H$	13.30	0	14.00	62.7	[9]
60	$C_8H_2 + C_4H^{\cdot} \rightleftharpoons C_{10}H_2 + C_2H^{\cdot}$	13.48	135.0	14.00	0	[9]

Table 2. (Contd.)

No.	Reaction	Rate constant				References
		forward reaction		reverse reaction		
		log$A$	E_a, kJ/mol	log$A$	E_a, kJ/mol	
61	$C_8H_2 + C_4H^{\bullet} \rightleftharpoons C_{12}H_2 + H$	13.60	0	14.00	66.0	[9]
62	$C_8H_2 + C_4H_3^{\bullet} \rightleftharpoons C_8H^{\bullet} + C_4H_4$	13.30	83.6	12.68	–59.4	"
63	$C_8H_2 + C_6H^{\bullet} \rightleftharpoons C_{14}H_2 + H$	13.00	0	14.00	66.0	"
64	$C_8H^{\bullet} + C_2H_2 \rightleftharpoons C_{10}H_2 + H$	13.60	0	14.00	66.0	"
65	$C_8H^{\bullet} + C_4H_2 \rightleftharpoons C_{12}H_2 + H$	13.60	0	14.00	66.0	"
66	$C_8H^{\bullet} + C_6H_2 \rightleftharpoons C_{14}H_2 + H$	13.00	0	14.00	66.0	"
67	$C_{10}H_4 + M \rightleftharpoons C_{10}H_2 + H_2 + M$	17.70	209.0	14.48	0	Estimate
68	$C_{10}H_2 \rightleftharpoons C_{10}H^{\bullet} + H$	14.90	502.0	13.43	30.1	[9]
69	$C_{10}H_2 + H \rightleftharpoons C_{10}H^{\bullet} + H_2$	14.00	86.9	13.30	0	"
70	$C_{10}H_2 + C_2H^{\bullet} \rightleftharpoons C_{10}H^{\bullet} + C_2H_2$	13.51	–47.3	13.60	0	"
71	$C_{10}H_2 + C_4H_3^{\bullet} \rightleftharpoons C_{10}H^{\bullet} + C_4H_4$	13.30	83.6	12.37	0	"
72	$C_{10}H_2 + C_2H^{\bullet} \rightleftharpoons C_{12}H_2 + H$	13.30	0	14.00	62.7	"
73	$C_{10}H_2 + C_4H^{\bullet} \rightleftharpoons C_{12}H_2 + C_2H^{\bullet}$	13.48	135.0	14.00	0	"
74	$C_{10}H_2 + C_4H^{\bullet} \rightleftharpoons C_{14}H_2 + H$	13.30	0	14.00	66.0	"
75	$C_{10}H^{\bullet} + C_2H_2 \rightleftharpoons C_{12}H_2 + H$	13.60	0	14.00	66.0	"
76	$C_{10}H^{\bullet} + C_4H_2 \rightleftharpoons C_{14}H_2 + H$	13.30	0	14.00	66.0	"
77	$C_{12}H_4 + M \rightleftharpoons C_{12}H_2 + H_2 + M$	17.70	188.0	14.48	0	Estimate
78	$C_{12}H_2 \rightleftharpoons C_{12}H^{\bullet} + H$	14.90	502.0	13.43	30.1	[9]
79	$C_{12}H_2 + H \rightleftharpoons C_{12}H^{\bullet} + H_2$	14.00	86.9	13.30	0	"
80	$C_{12}H_2 + C_4H_3^{\bullet} \rightleftharpoons C_{12}H^{\bullet} + C_4H_4$	13.30	83.6	12.37	18.6	"
81	$C_{12}H_2 + C_2H^{\bullet} \rightleftharpoons C_{12}H^{\bullet} + C_2H_2$	13.51	–47.3	13.60	0	"
82	$C_{12}H_2 + C_2H^{\bullet} \rightleftharpoons C_{14}H_2 + H$	13.30	0	14.00	62.7	"
83	$C_{12}H^{\bullet} + C_2H_2 \rightleftharpoons C_{14}H_2 + H$	13.60	0	14.00	66.0	"
84	$C_{14}H_4 + M \rightleftharpoons C_{14}H_2 + H_2 + M$	17.70	188.0	14.48	0	Estimate
85	$H_2 + M \rightleftharpoons H + H + M$	15.11	423.0	14.49	–13.1	[31]
86	$C_{10}H_2 + C_{10}H_2 \longrightarrow Z + H_2 + H_2$	12.81	0	–	–	[9]
87	$C_{12}H_2 + C_8H_2 \longrightarrow Z + H_2 + H_2$	12.81	0	–	–	"
88	$C_{12}H_2 + C_{10}H_2 \longrightarrow Z + H_2 + H_2$	12.81	0	–	–	"
89	$C_{12}H_2 + C_{12}H_2 \longrightarrow Z + H_2 + H_2$	12.81	0	–	–	"
90	$C_{14}H_2 + C_6H_2 \longrightarrow Z + H_2 + H_2$	12.81	0	–	–	"
91	$C_{14}H_2 + C_8H_2 \longrightarrow Z + H_2 + H_2$	12.81	0	–	–	"
92	$C_{14}H_2 + C_{10}H_2 \longrightarrow Z + H_2 + H_2$	12.81	0	–	–	"

Table 2. (Contd.)

No.	Reaction	Rate constant				References
		forward reaction		reverse reaction		
		log$A$	E_a, kJ/mol	log$A$	E_a, kJ/mol	
93	$C_{14}H_2 + C_{12}H_2 \longrightarrow Z + H_2 + H_2$	12.81	0	–	–	Estimate
94	$C_{14}H_2 + C_{14}H_2 \longrightarrow Z + H_2 + H_2$	12.81	0	–	–	"
95	$Z + C_2H_2 + M \rightleftharpoons Z + H_2 + M$	13.72	0	28.84	577.0	"
96	$Z + C_2H^{\cdot} + M \rightleftharpoons Z + H + M$	13.74	0	28.86	577.0	"
97	$Z + C_4H_2 \rightleftharpoons Z + H_2$	11.48	0	10.30	10.3	"
98	$Z + C_4H^{\cdot} \rightleftharpoons Z + H$	11.48	0	13.30	446.0	"
99	$Z + C_6H_2 \longrightarrow Z + H_2$	9.70	0	–	–	"
100	$Z + C_6H^{\cdot} \longrightarrow Z + H$	9.70	0	–	–	"
101	$Z + C_8H_2 \longrightarrow Z + H_2$	9.70	0	–	–	"
102	$Z + C_8H^{\cdot} \longrightarrow Z + H$	9.70	0	–	–	"
103	$Z + C_{10}H_2 \longrightarrow Z + H_2$	9.70	0	–	–	"
104	$Z + C_{10}H^{\cdot} \longrightarrow Z + H$	9.70	0	–	–	"
105	$Z + C_{12}H_2 \longrightarrow Z + H_2$	9.70	0	–	–	"
106	$Z + C_{12}H^{\cdot} \longrightarrow Z + H$	9.70	0	–	–	"
107	$Z + C_{14}H_2 \longrightarrow Z + H_2$	9.70	0	–	–	"
108	$Z + C_4H_4 \longrightarrow Z + H_2 + H_2$	9.70	0	–	–	"
109	$Z + C_2H^{\cdot} \rightleftharpoons Z + C_4H^{\cdot}$	13.30	184.0	11.48	0	"
110	$Z + C_2H_2 \rightleftharpoons Z + C_4H_2$	13.30	182.0	11.48	0	"
111	$Z + Z \longrightarrow Z$	12.65	0	–	–	"

Note: The rate constants are described in the form $k = A\exp(-E_a/RT)$ in mol, cm^3, and s.
The rate constants for reactions with Z as a reactant are proportional to the frequency of collisions and change with a growth of the average size M_Z of soot particles. This was taken into account by multiplying the values cited in the table by $T^{1/2}B^{1/2}M_Z^{2/3}$ (for reactions 95–110 or by $T^{1/2}M_Z^{1/6}$ for reaction 111), where B is the number of carbon atoms that transfer from the gas into the solid phase or backward.

We also included reactions that are the reverse of (II) and (III) for n = 1 and 2. The occurrence of reverse reactions enabled us to determine the equilibrium yield of soot. In addition to other reactions, we included in the model of soot formation the step that describes the process of soot particle coagulation in a simplified form:

$$Z + Z \longrightarrow Z. \qquad \text{(IV)}$$

Thus, the weight of carbon in the condensed phase changes in reactions (I)–(III), and the concentration of particles changes in reactions (I) and (IV). If the rates of these processes are known, the changes of the average size of soot particles can be calculated.

The rate constants for reactions responsible for the formation of soot particles, their growth, and their destruction (reactions 86–111 from Table 2) were fitted to experimental data. Clearly, these reactions are not elementary and describe several physical and chemical processes.

Determination of the heat of formation for soot particles. To reveal thermal factors that affect the kinetics of soot formation, it was necessary to determine the thermodynamic parameters of soot particles formed in the reaction. The determination of soot formation heat should be considered separately.

Wang and Frenklach [14] analyzed the formation heats for polyaromatic molecules and benzenoid radi-

cals calculated by different methods (group method, semiempirical molecular dynamics simulations, and quantum mechanics). These data were compared to the experimental data for various substances [15]. Wang and Frenklach proposed the methods for calculating the heats of formation using a combination of quantum-mechanical and group methods. The values of the heats of formation per one carbon atom are 11.5–16.0 kJ/mol for coronene (depending on the calculation method) and 6.3–11.8 kJ/mol for large molecules (H/C → 0). The experimental data have been only found for medium-sized substances (up to perylene, whose formation heat is 16.5 kJ/mol). The calculation results for large molecules strongly depend on the method.

Our analysis of the experimental temperature dependence of the soot yield in *n*-hexane pyrolysis at various pressures [16] suggested that the heat of soot formation can be estimated by a method other than those considered in [14]. It is important that experiments reported in [16] were carried out using the same setup and the same method for soot measurements as in this work.

The main idea that forms the basis for the method discussed below is to describe a shift of the bell-shaped curve of soot yield in a temperature scale depending on the molar fraction of the hydrocarbon in the starting mixture with argon. This effect is most pronounced in experiments with *n*-hexane [16] and *n*-heptane [17]. In the experiment with ethylene, the shift is small. This is because the process of soot formation in ethylene is virtually thermoneutral. Therefore, we did not expect any noticeable shift in the case of ethylene. The shift is more pronounced for *n*-hexane comparatively to *n*-heptane [17]. In our opinion, there are two reasons for that. First, in the experiments with *n*-heptane, the mixture contained some amount of oxygen (with a stoichiometric coefficient of 5), which may substantially compensate for the heat loss during the decomposition of starting molecules by heat evolved in their partial oxidation. Second, the experiments with *n*-heptane were carried out in a tube with a small diameter (3.1 cm). Therefore, the gas-dynamic heating of gas is possible behind a reflected shock wave because of the turbulization of the boundary layer and the partial adiabatic compression of gas near the end of the tube. Therefore, we chose the experiments with *n*-hexane to estimate the heat of soot formation.

Open circles in Fig. 2 show the results of the measurements of soot yield in *n*-hexane pyrolysis for different pressures behind the shock waves. The concentration of *n*-hexane behind the front of a reflected shock wave was about the same in all the runs (~8.33×10^{-7} mol/cm^3). Each of three series of experiments forms its own bell-shaped curve, which is shifted toward higher temperatures when the pressure is lower (see Fig. 2). The maximum value of soot yield for each series is approximately the same (20–22%). Because the yield of soot is determined by the corresponding

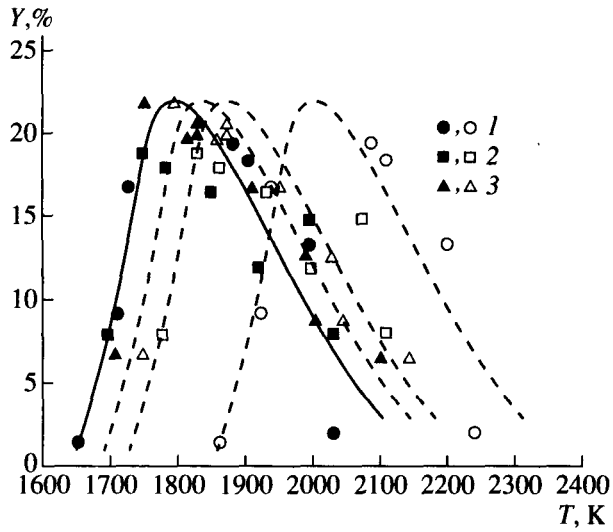

Fig. 2. Soot yield (Y) versus initial (open circles, triangles, squares; dashed lines) and final (solid circles, triangles, and squares; solid lines) temperatures of the mixture behind the shock waves in *n*-hexane pyrolysis at the (*1*) 25, (*2*) 50, and (*3*) 100 bar. The concentrations of *n*-C_6H_{14} are (*1*) 0.714, (*2*) 0.273, and (*3*) 0.144%.

thermodynamic conditions formed due to physicochemical processes in the mixture during pyrolysis, we may assume that, despite the differences in initial conditions, the final temperature of the mixtures in the points of maxima of bell-shaped curves is the same.

The experimental points shown in Fig. 2 refer to the initial temperature of the mixture without considering that the overall process is endothermic and the final temperature of the mixture is lower than the initial temperature. Considering that the relative shifts of bell-shaped curves are due to the nonisothermal nature of the process, let us estimate the apparent heat of soot formation.

Figure 2 shows bell-shaped curves for a series of experiments differing in pressure. The curves shift toward higher temperatures for a higher molar fraction at a constant concentration of *n*-hexane. Let us determine approximate maxima (T_{max}) for each mixture and construct a plot of these maxima versus the *n*-hexane molar fraction (N^0_{hex}/N^0_m) in the initial mixture (Fig. 3). The resulting dependence is approximated by a linear equation

$$T_{max} = 1793 + 29153 N^0_{hex}/N^0_m,$$

where N^0_m m is the initial concentration of molecules in the gas.

This result enables the estimation of the heat of soot formation per one carbon atom. Let us assume that soot particles contain 22% of the starting carbon (Fig. 2) and that the rest of carbon and the entire hydrogen remain in the gas phase and form hydrocarbon species, which are in local thermodynamic equilibria. Upon calculat-

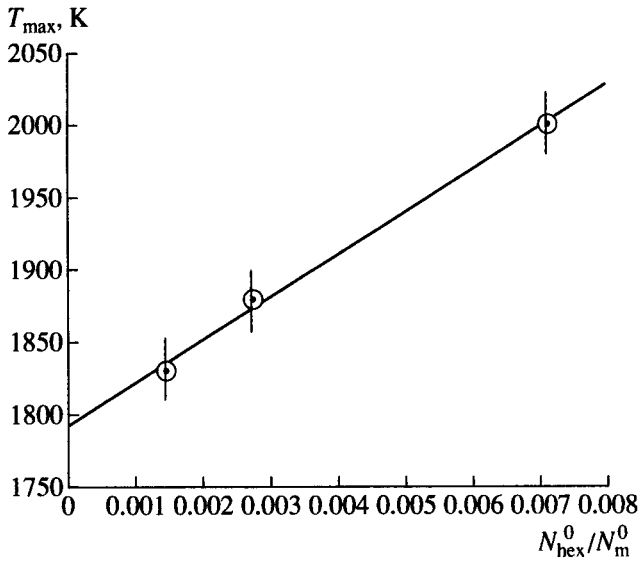

Fig. 3. Temperature of the maximal yield of soot versus *n*-hexane molar fraction in the initial mixture in the pyrolysis of *n*-hexane behind a shock wave at various pressures.

ing the final equilibrium composition of gas and knowing the composition of the starting mixture and initial and final temperatures, we may calculate the heat of the process and the heat of soot formation from the condition of heat balance

$$\Delta H_{T,Z} = \frac{N^0_{hex}\Delta H_{T,hex} + \sum_i N_i(\Delta H_{T,i} - \Delta TC_i)}{N_{CZ}}, \quad (1)$$

where $\Delta H_{T,hex}$ is the enthalpy of *n*-hexane formation at $T = 1793$ K; $\Delta H_{T,i}$, N_i, and C_i are the enthalpy of formation, equilibrium concentration, and heat capacity of species that are taken into account in the calculation of the equilibrium composition of the final gaseous mixture; ΔT is a change in the temperature of mixture after the reaction; and N_{CZ} is the concentration of carbon atoms accumulated in soot particles.

The equilibrium composition of the gas is calculated from the balance condition with respect to carbon and hydrogen atoms. Thermodynamic equilibrium constants for the species [18] were used corresponding to the conditions of the maximum yield of soot, taking into account a shift in the temperature: $T = 1793$ K, the initial concentration of *n*-hexane is $N^0_{hex} = 8.33 \times 10^{-7}$ mol/cm^3, and the yield of soot is $Y = 22\%$. In this calculation, we assumed that the gas contains only small molecules and radicals containing up to four carbon atoms. We calculated the equilibrium composition taking into account the species containing at most two, three, and four carbon atoms. The results of calculation show that, with an increase in the number of species under consideration, the values of $\Delta H_{T,Z}$ increase: –5 kJ/mol for C_2; 23 kJ/mol for C_2- and C_3; and 26 kJ/mol for C_4. As can be seen, the value of $\Delta H_{T,Z}$ obtained when C_3 species are taken into account differs substantially from the values obtained when only C_2 species are taken into account. However, a further increase in the number of species that are taken into account, the $\Delta H_{T,Z}$ value remains virtually the same. Therefore, it is reasonable to assume the estimated value $\Delta H_{T,Z} = 26$ kJ/mol. Because the error in determining ΔT is about ±20 K (see Fig. 2), the error in determining the maximum yield of soot is ~20%, and the error in determining $\Delta H_{T,Z}$ associated with the inaccuracy in the equilibrium composition of the gas phase is ~2 kJ/mol, we obtain from equation (1) that the error in determining $\Delta H_{T,Z}$ is ±6 kJ/mol. Thus, $\Delta H_{T,Z} = 26 \pm 6$ kJ/mol. Using the data on the heat capacity of gaseous graphite [18], we obtain the value of the standard heat of soot formation $\Delta H_{f,Z} = 11 \pm 6$ kJ/mol. This value correlates well with the results of the earlier calculation [14].

Using the value $\Delta H_{f,Z} = 11$ kJ/mol, we calculated the final temperature for each of the experimental points in Fig. 2 using the method described above. Figure 2 shows the dependence of the soot yield on the final temperature of the mixture (solid circles). It is seen that the results of soot yield measurements for different pressures form a unified dependence on the final temperature of the mixture.

Calculation of the temperature of soot particles. The complete description of the energetic characteristics of the particles should be based on solving the set of macrokinetic equations for the nonequilibrium energy distribution (ED) function, taking into account that, in the condensation process, the size distribution (SD) function of particles is also formed. In practice, finding a solution for the two-dimensional distribution function is very difficult. Considering current capabilities in describing the nonequilibrium effects in kinetic processes involving microparticles, the best results can be obtained if the apparent vibratory temperature for medium-sized particles is used. The use of vibratory temperature has approved itself in molecular and chemical kinetics [11, 12]. Also, Monte Carlo calculations [13] point to the fact that, for the particle, one can introduce some apparent temperature T_{app} (which, in fact, should be considered the vibratory temperature); that is, a particle has Boltzmannian ED and its temperature differs from that of the gas phase.

The calculation of the average size of soot particles using the methods of formal kinetics is easy. For that, it is enough to introduce the equations for the concentration of soot particles and carbon atoms which enter the composition of these particles into the set of the differential equations of chemical kinetics. From the standpoint of formal kinetics, soot particles are not different from other components (molecules, radicals, and atoms) of the kinetic scheme. The corresponding differential equation can be written in a usual form taking into account the number of carbon atoms that transfer

into the condensed phase and back to the gas phase in reactions (I)–(III) or similar reactions.

To estimate the temperature of soot particles, let us consider their energetic balance, which accounts for heat fluxes associated with the reactions of particle growth and destruction and energy exchange with the atoms of ambient gas.

The main physical parameter that characterizes the process of energy exchange is the value of the average energy that transfers in a collision $\overline{\Delta E}$. This parameter can be estimated using the statistical theory of unimolecular reactions [19, 20]. This approach considers soot particles as quasimolecular entities with corresponding ED [11, 21–24]. This function is formed due to competing chemical processes resulting in the deterioration of equilibrium ED and energy exchange in collisions with the atoms of a buffer gas, which recovers its deteriorated equilibrium.

To carry out this calculation within the framework of statistical theory, it is necessary to know the number of vibratory energetic states for a particle $W(E)$ in the interval $[0, E]$ and their density depending on the excitation energy $\rho(E)$. Strict determination of these functions requires summing over the whole spectrum of the vibratory frequencies of a particle. In the simplest case, when $E \gg h\omega$ (quasiclassical approach), the number of energetic states for the vibratory motion of a molecule is adequately approximated by the equation

$$W(E) = AE^s,$$

where s is the number of vibratory modes. We will further use this formula and the corresponding expression for the state density

$$\rho(E) = \frac{dW(E)}{dE} = sAE^{s-1}.$$

The statistical model [25–29] of energy exchange implies that, during collision, a collisional complex is formed whose lifetime is long enough for the randomization of its energetic states. Upon the decomposition of this complex, energy is randomly distributed according to statistic weights of various degrees of freedom of products. If before the collision, the internal energy of the species is E_0 and the kinetic energy of collision is E_θ, then the probability $p(\Delta E)$ of a change in the internal energy of the species is ΔE ($-E_0 < \Delta E < E_\theta$) equal to

$$p(\Delta E) = \frac{\int_{-E_0}^{\Delta E} (E_0 + x)^{s-1}(E_\theta - x)^{\theta/2-1}dx}{\int_{-E_0}^{E_\theta} (E_0 + x)^{s-1}(E_\theta - x)^{\theta/2-1}dx},$$

where θ is the number of degrees of freedom of the translational motion of species participating in the collision (in the general case, $\theta = 4$). Upon integration, we have

$$p(\Delta E) = \varepsilon^s(1 + s - s\varepsilon), \quad \varepsilon = \frac{E_0 + \Delta E}{E_0 + E_\theta}.$$

The probability density (the distribution function) of an energy change during collision is

$$F(\Delta E) = \frac{dp(\Delta E)}{d\Delta E} = \frac{s(s+1)}{E_0 + E_\theta}\varepsilon^{s-1}(1 - \varepsilon).$$

The average change in the energy and the average square of the energy change during collision with energy E_θ are

$$\langle \Delta E \rangle = \int_{-E_0}^{E_\theta} \Delta E F(\Delta E) d\Delta E = \frac{sE_\theta - 2E_0}{s+2}.$$

Upon averaging these expressions according to the Maxwell distribution function over collision energies $F_\theta = (RT)^{-1}E_\theta \exp(-E_\theta/RT)$, we have

$$\overline{\Delta E} = RT\frac{s - \Theta}{1 + s/2},$$

$$\Theta = E_0/RT.$$

If the apparent temperature of a particle is T_Z and the gas temperature is T_g, then $\Theta = sT_Z/T_g$ at high values of s, and the average energy transferred during collisions is $\overline{\Delta E} = 2R(T_g - T_Z)$. The temperature of particles changes because of vibratory–translational relaxation at the rate

$$\left(\frac{dT_Z}{dt}\right)_{VT} = \frac{2\alpha\sigma v_{av}N_m}{3M_Z}(T_g + T_Z), \qquad (2)$$

where $\sigma = \pi r_0^2 M_Z^{2/3}$ is the collision cross-section of soot particles with the gas molecules; M_Z is the number of carbon atoms in a particle; r_0 is the average size per one carbon atom in a particle; $v_{av} = (8\pi kT_g/\mu)^{1/2}$ is the average heat rate, μ is the apparent mass; N_m is the concentration of molecules in the gas phase; and α is the coefficient of collision efficiency.

Intramolecular vibratory energy exchange during collision is usually incomplete. That is, during collision, not all of the modes of a particle take part in the process of energy redistribution over the degrees of freedom, and statistical theories should be modified. Therefore, to describe the process of energy exchange in the case of complex polyatomic molecules and particles, the local model of the statistical complex [28] is used, which assumes that statistical equilibrium is attained for the separate low-frequency vibratory and rotational degrees of freedom of a collisional complex [12]. The distribution of energy over other degrees of freedom of a molecule occurs between collisions. This model leads to rather complex expressions, and, in the general case, it requires the correct consideration of the

interactions between separate vibratory modes of a molecule or a particle. Because information on the interactions between modes is associated with substantial uncertainties, we restricted ourselves to introducing the coefficient α into expression (2). This empirical coefficient accounts for the probability of collisions without energy exchange.

Another component that determines a change in the apparent temperature of particles is the occurrence of the chemical reactions of growth or destruction of soot particles. A "chemical" term in the equation for a change in the temperature of soot particles has the following form:

$$\left(\frac{dT_Z}{dt}\right)_{chem} = \frac{\beta\sum_i w_i Q_i}{3RN_{CZ}},$$

where w_i and Q_i are the rates and heats of reactions (I)–(IV) involving soot particles; β is an empirical coefficient that accounts for the fraction of energy evolved in the chemical reactions and remaining on the vibratory degrees of freedom; and N_{CZ} is the concentration of carbon atoms in the condensed state.

The complete set of equations, which models the kinetics of soot formation, involves equations that describe changes in the concentrations N_i ($i = 1, \ldots, n_p$) of reacting components:

$$\frac{dN_i}{dt} = \sum_{j=1}^{n_r} w_j \eta_{ij},$$

where n_p is the number of components participating in the process, including soot particles and carbon atoms entering their composition; n_r is the number of reactions in the scheme (Table 2); w_j is the rate of the jth reaction; and n_{ij} is the stoichiometric coefficient of the ith component in the jth reaction. In the equation for the concentration of carbon atoms in the composition of soot particles, the stoichiometric coefficient equals the number (with a positive sign) of carbon atoms that transfer from the gas to the condensed phase due to the reaction. The negative sign corresponds to the reverse process. The set of equations also contains the equation for soot particle temperature

$$\frac{dT_Z}{dt} = \left(\frac{dT_Z}{dt}\right)_{chem} + \left(\frac{dT_Z}{dt}\right)_{VT}, \quad (3)$$

and gas temperature

$$\frac{dT_g}{dt} = \frac{(1-\beta)\sum_{j=1}^{n_r} w_j Q_j - 3RN_{CZ}\left(\frac{dT_Z}{dt}\right)_{VT}}{\sum_{i=1}^{n_p} C_i N_i}, \quad (4)$$

where C_i is the heat capacity of the ith component of the mixture.

The rate constants of forward and reverse reactions involved in the kinetic scheme are listed in Table 2 in the Arrhenius form $k = A\exp(-E_a/RT)$. We assumed that for the reactions where soot particles are reactants, the rate constants are proportional to the frequency of collisions and change with a change in the particle size. The preexponential factors for reactions 95–111 from Table 2 were multiplied by the current values of $(N_{CZ}/N_Z)^{2/3}T_g^{1/2}$.

An important component of this model is the dependence of the rate constant for particle destruction (reverse reactions 95–98, 109, and 110) on the temperature of particles T_Z: $k = A\exp(-E_a/RT_Z)$.

Note that equation (3) for the temperature of particles describes to a first approximation the balance of energy formed in the exothermic processes of apparent particle Z growth, the reverse endothermic reactions, and the processes of vibratory cluster–gas energy exchange (V–T relaxation). A more complete and difficult task is the description of the structural transformation of soot particles in the process of their growth, taking into account the energetics of this process. In most cases, the reaction rates of the structural transformation of particles are sensitive to a reserve of the vibratory energy of particles.

CALCULATION RESULTS AND DISCUSSION

The calculation of the kinetics of soot formation was carried out for ethylene pyrolysis at a pressure of 50 bar and initial temperatures of 1700–2200 K. A mixture of C_2H_4 (0.66%) in argon was studied. The experimental data used for simulating the kinetic scheme were obtained in reflected shock waves in a setup described in [16] using the method of light absorption at a wavelength of He–Ne laser irradiation of $\lambda = 632.8$ nm.

Figure 4 shows the calculated dependence of soot yield on time for various initial temperatures along with the experimental dependences obtained under comparable conditions. Figure 5 shows the calculated and experimental dependences of soot yield on the initial temperature of the mixture by the time $t = 1$ ms.

The greatest attention in calculation was paid to changes in the temperatures of gas and particles during the process. Figure 6a shows the calculated curves for the temperatures of gas phase and soot particles. A drastic decrease in the temperature is initially observed, which is associated with the endothermicity of ethylene decomposition. The amplitude of a temperature decrease is 50–100 K, depending on the initial temperature. Then, the temperature somewhat increases and reaches the equilibrium level. The temperature of soot particles is noticeably higher than the gas temperature. The highest temperature difference is observed during

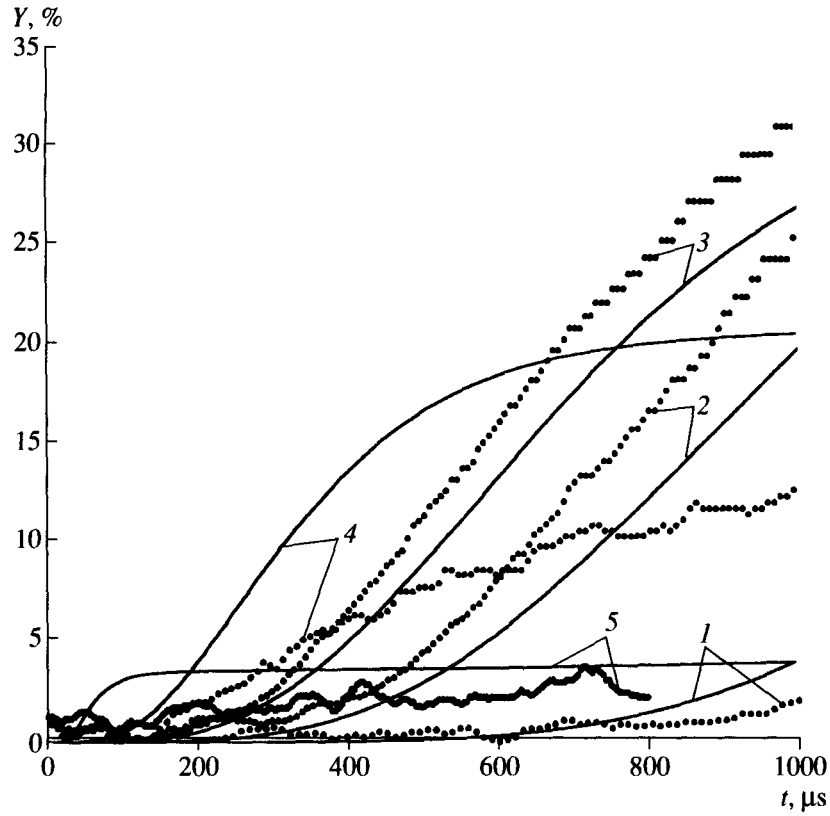

Fig. 4. Soot yield versus time for various temperatures of the mixture behind shock waves: (*1*) 1733, (*2*) 1839, (*3*) 1903, (*4*) 2003, and (*5*) 2166 K. Dashed lines represent the experiment and solid lines represent the calculation.

intensive soot formation. By the end of the process, the temperatures of particles and gas become the same. Within the framework of the model adopted here, the factor that determines the temperature gradient between particles and gas is the coefficient α, which characterizes the efficiency of energy exchange between particles and ambient gas. Figure 6b shows a change in the profile of particle temperatures when varying the coefficient α from 0.1 to 0.001 (at $\alpha = 1$, the difference between temperatures is virtually absent).

To find out if the model that describes the growth of soot particles and the evolution of particle and gas temperatures is adequate to the experiment, we should compare the calculation to the experimental data on the temperature of particles in hydrocarbon pyrolysis. We are planning to supplement the "temperature" equation with the terms to account for structural transformation and corresponding energetics and discuss this problem elsewhere.

When modeling the processes of condensed phase formation during gas-phase reactions, including soot formation, it is necessary to pay attention to the dynamics of particle size. In the general case, during these processes, the function of condensed-phase particle distribution over sizes is formed. It is rather difficult to determine the dynamics of parameters of this distribution function either experimentally or theoretically. A change in the size of particles is due to the initiation and monomer addition reactions and coagulation processes. In several papers, this problem was discussed using a starting point of various model systems for the

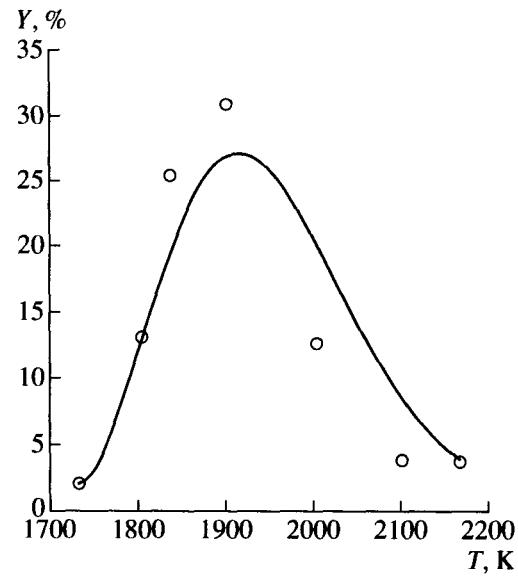

Fig. 5. Soot yield by the time $t = 1$ ms versus the initial temperature behind the front of a reflected shock wave for the 0.66% C_2H_4/Ar mixture at 50 bar. Points represent the experiment and the line represents the calculation.

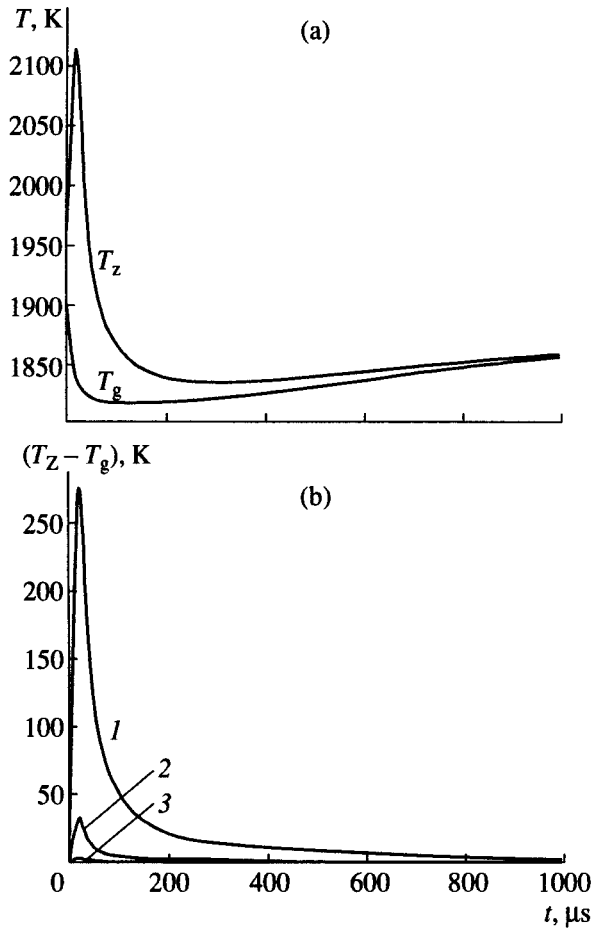

Fig. 6. (a) Temperature profile of gas T_g and soot particles T_Z ($\alpha = 0.001$) and (b) their difference at different values of the α parameter: (*1*) 0.001, (*2*) 0.01, and (*3*) 0.1.

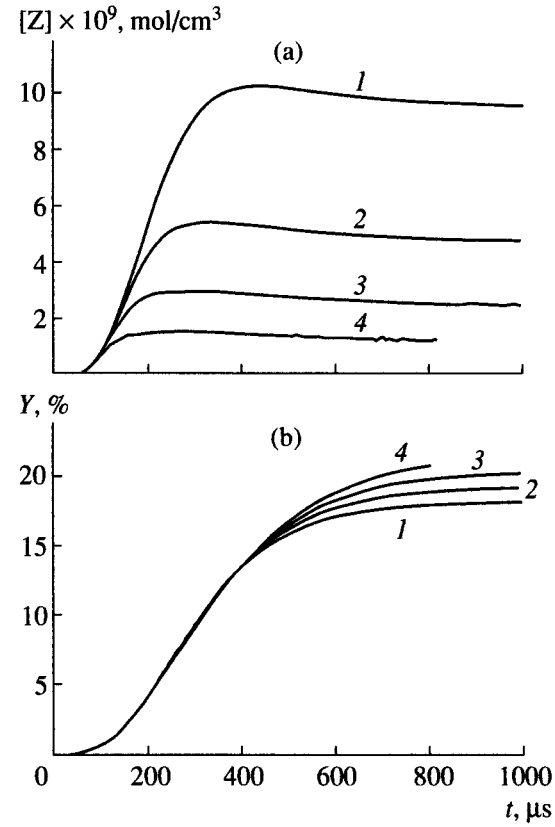

Fig. 7. (a) Calculated concentrations of soot particles and (b) soot yield at different values of the rate constants of the reaction Z + Z ⟶ Z: (*1*) 4.5×10^{11}, (*2*) 1.5×10^{12}, (*3*) 4.5×10^{12}, and (*4*) 1.5×10^{13} cm^3 mol^{-1} s^{-1} (the 0.66% C_2H_4/Ar mixture, 2003 K, 50 bar).

condensation of supersaturated metal vapors formed behind shock waves as a result of the decomposition of metal-containing compounds [22, 30]. The data on the changes of soot particle size and concentrations in pyrolysis are very scarce [17]. In the kinetic scheme considered above (Table 2), this problem is solved within the framework of monodispersed approximation. Coagulation processes occurring in the system are modeled with the apparent reaction Z + Z ⟶ Z. Figure 7 shows how the concentration of soot particles and the yield Y of soot change depending on the value of the rate constant of this reaction. As can be seen, the value of this rate constant does not substantially affect the yield of soot, but it does affect the concentration and size of particles.

This result suggests that a more detailed description of coagulation in the general set of equations is not the first-priority task in the description of the above integral characteristics (Y and k_{eff}) of the soot formation process in shock waves.

As can be seen, the results of calculation describe the main characteristic features of soot formation, such as the presence of the *S*-shaped profile of soot concentration with a pronounced induction period and the formation of a volcano-shaped plot for soot yield versus initial temperature. This lets us conclude that soot formation via polyyine molecules, which forms the basis of our model, may be considered as one of the most probable mechanisms along with HACA and other mechanisms. The formation and growth of soot particles probably occurs via different pathways: via polyyne chains or polyaromatic compounds. Depending on the conditions for soot formation, gas-phase composition, and process stage, one of the mechanisms may dominate over others. However, in the general case, soot formation is a complex process which may occur via different pathways.

An important aspect of soot formation modeling is an account of unsteady temperature, which reveals itself during the process. It is necessary to take into account both a change in the gas temperature and the temperature of soot particles. The knowledge of particle temperature is necessary for interpreting optical measurements and describing the kinetics of soot formation. The dynamics of temperature during the process is especially important when modeling the processes of the structure formation of soot particles. In

this work, we did not discuss this important aspect. Obviously, the temperature of soot particles rather than the gas-phase temperature determines the process of their structure formation.

ACKNOWLEDGMENTS

This work was supported by the Russian Foundation for Basic Research (project nos. 96-03-33611 and 98-03-32157).

REFERENCES

1. Haynes, B.S., Jander, H., Matzig, H., and Wagner, H.Gg., *19th Int. Symp. on Combustion*, Pittsburgh: The Combustion Institute, 1982, p. 1379.
2. Haynes, B.S. and Wagner, H.Gg., *Prog. Energy Combust. Sci.*, 1981, vol. 7, no. 11, p. 2293.
3. Warnatz, J., Maas, U., and Dibble, R.W., *Combustion*, Heidelberg: Springer, 1996.
4. Bauerle, St., Karasevich, Yu., Slavov, St., *et al., 25th Int. Symp. on Combustion*, Pittsburgh: The Combustion Institute, 1994, p. 627.
5. Starikovsky, A.Yu., Thienel, Th., Wagner, H.Gg., and Zaslonko, I.S., *Ber. Bunsen-Ges. Phys. Chem.*, 1998, vol. 102, no. 12, p. 1815.
6. Frenklach, M., Hsu, J.P., Miller, D.L., and Matula, R.A., *Combust. Flame*, 1986, vol. 64, no. 1, p. 141.
7. Karlov, N.V., Kirichenko, N.A., and Luk'yanchuk, B.S., *Lazernaya termokhimiya* (Laser Thermochemistry), Moscow: Tsentrkom, 1995.
8. Frenklach, M., *Chem. Eng. Sci.*, 1985, vol. 40, no. 9, p. 1843.
9. Krestinin, A.V., *Khim. Fiz.*, 1994, vol. 13, no. 1, p. 121.
10. Warnatz, J., Behrendt, F., Sojka, J., *et al.*, *Advanced Computation and Analysis of Combustion*, Roy, G.D., Frolov, S.M., and Givi, P., Eds., Moscow: ENAS, 1997, p. 64.
11. Zaslonko, I.S., *Doctoral (Phys.–Math.) Dissertation*, Moscow: Inst. of Chem. Phys., 1981.
12. Kuznetsov, N.M., *Kinetika monomolekulyarnykh reaktsii* (Kinetics of Unimolecular Reactions), Moscow: Nauka, 1982.
13. Vlasov, P.A., Karasevich, Yu.K., and Smirnov, V.N., *Teplofiz. Vys. Temp.*, 1996, vol. 34, no. 5, p. 676.
14. Wang, H. and Frenklach, M., *J. Phys. Chem.*, 1993, vol. 97, no. 15, p. 3867.
15. Pedley, J.B., Naylor, R.D., and Kirby, S.P., *Thermochemical Data of Organic Compounds*, London: Chapman and Hall, 1986.
16. Hwang, S.M., Vlasov, P., Wagner, H.Gg., and Wolff, Th., *Z. Phys. Chemie, Neue Folge*, 1991, vol. 173, no. 1, p. 129.
17. Kellerer, H., Muller, A., Bauer, H.-J., and Wittig, S., *Combust. Sci. Technol.*, 1996, vol. 113–114, no. 1, p. 67.
18. Burcat, A., *Combustion Chemistry*, Gardiner, W.C., Jr., Ed., New York: Springer, 1984, p. 455.
19. Robinson, P. and Hallbrook, C., *Unimolecular Reactions*, New York: Wiley, 1975.
20. Forst, W., *Theory of Unimolecular Reactions*, London: Academic, 1973.
21. Lian, L., Su, C.-X., and Armentrout, P.B., *J. Chem. Phys.*, 1992, vol. 97, no. 5, p. 4072.
22. Freund, H.J. and Bauer, S.H., *J. Phys. Chem.*, 1977, vol. 81, no. 10, p. 1015.
23. Gordiets, B.V., Shelepin, L.A., and Shmotkin, Yu.S., *Khim. Fiz.*, 1982, no. 10, p. 1391.
24. Jarrold, M.F., *J. Phys. Chem.*, 1995, vol. 99, no. 1, p. 11.
25. Keck, J. and Kalelkar, A., *J. Chem. Phys.*, 1968, vol. 49, no. 7, p. 3211.
26. Nordholm, S., Freaser, B.S., and Jolly, I.L., *J. Chem. Phys.*, 1977, vol. 25, no. 3, p. 433.
27. Egorov, V.V. and Kuznetsov, N.M., *Dokl. Akad. Nauk SSSR*, 1980, vol. 252, no. 6, p. 1421.
28. Kuznetsov, N.M. and Egorov, V.V., *Dokl. Akad. Nauk SSSR*, 1980, vol. 255, no. 2, p. 380.
29. Egorov, V.V. and Kuznetsov, N.M., *Dokl. Akad. Nauk SSSR*, 1981, vol. 258, no. 6, p. 1396.
30. Vlasov, P.A., Zaslonko, I.S., Karasevich, Yu.K., and Lidskii, B.V., *Teplofiz. Vys. Temp.*, 1997, vol. 35, no. 6, p. 947.
31. Mallard, W.G., Westley, F., Herron, J.T., and Hampson, R.F., *NIST Standard Reference Data*, Gaithersburg: NIST, 1994.
32. Just, Th., Roth, P., and Damm, R., *Int. Symp. on Combustion Proc.*, 1977, vol. 16, p. 961.
33. Warnatz, J., *Combustion Chemistry*, Gardiner, W.C., Jr., Ed., New York: Springer, 1984, p. 197.
34. Kiefer, J.H. and von Drasek, W.A., *Int. J. Chem. Kinet.*, 1990, vol. 22, no. 7, p. 747.
35. Schulz, G., Klotz, H.-D., and Spangenberg, H.-J., *Z. Chem.*, 1985, vol. 25, no. 1, p. 88.
36. Frank, P. and Just, Th., *Int. Symp. on Shock Tubes Proc.*, 1984, vol. 14, p. 706.
37. Tsang, W. and Hampson, R.F., *J. Phys. Chem. Ref. Data*, 1986, vol. 15, no. 3, p. 1087.
38. Tanzawa, T. and Gardiner, W.C., *J. Phys. Chem.*, 1980, vol. 84, no. 2, p. 236.
39. Baulch, D.L., Cobos, C.J., Cox, R.A., *et al., J. Phys. Chem., Ref. Data*, 1992, vol. 21, no. 2, p. 411.
40. Ghibaudi, E. and Colussi, A.J., *J. Phys. Chem.*, 1988, vol. 92, no. 24, p. 5839.